Real time FT-IR observation of materials during their cooling from molten state

I.M. Ermini, L. Cosson, F. Fayon, D. Zanghi, C. Tardivat, D. de Sousa Meneses

Real time FT-IR observation of materials during their cooling from molten state

I.M. Ermini[a,c,*], L. Cosson[a], F. Fayon[a], D. Zanghi[a], C. Tardivat[b], D. De Sousa Meneses[a]

[a] CNRS, CEMHTI UPR3079, Univ. Orléans, F-45071 Orléans, France
[b] LSFC, UMR 3080 CNRS/Saint-Gobain CREE, Saint-Gobain Research Provence, 550 avenue Alphonse Jauffret, Cavaillon, France
[c] LABORATOIRE COMMUN CANOPEE, CNRS /Université de Lorraine / Saint-Gobain

[*] Corresponding Author

November 4, 2022

Abstract

A new methodology allowing real time observation of materials during their cooling, from the molten state to low temperature has been developed. This possibility originates from the implementation of a Rapid Scan feature on a FT-IR emissometer designed to probe materials submitted to extreme temperature conditions. Original time-resolved emissivity dependence during the phase transition are reported for the first time. The resulting out of equilibrium, dynamic, new data have been compared to the equilibrium, static, classical measurements to demonstrate the reliability of the new technique on two reference samples (Al_2O_3 and SiO_2). The proposed method has high possibilities to be applied to different materials to enable the observation of fast structural transformations during liquid to solid phase change through the evolution of the dielectric function.

Keywords

Real time FT-IR
Material emissivity
High temperature
Reflectance spectra
Solidification process

1 Introduction

The quest for high speed data acquisition is still ongoing [1] due to the necessity of instrumentation improvement to be able to observe fast occurring phenomena [2] such as phase transitions [3] or changes in microstructures [4]. This is of particular interest in the case of high temperature processes that involve, most of the time, transient states, metastable or out of equilibrium phases during cooling and which concerns many large scale industrial production such as glass and ceramics manufacturing. Different techniques have been used to probe in-situ the evolution of the microstructure in the liquid phase as the temperature is reduced, and different information can be obtained, making these techniques complementary to one another. For example, one can mention the use of X-ray [5, 6] or neutron diffraction [7] which provide information about coordination numbers and interatomic distances through the radial distribution function. In all of these cases, high-flux sources such as syncrotron radiation are needed in order to perform the experiments at high speed. Time-resolved ^{27}Al high temperature Nuclear Magnetic Resonance (NMR) has also been used to study in-situ solidification of alumina [8] and strontium aluminosilicates [7] for example. However, such NMR experiments require to target a nucleus of high NMR-sensitivity which is not always possible and restricts the applications of the method.

FT-IR emissivity measurements have not yet been widely used to study the structure and dynamics of materials at high temperatures. However, this technique allows to obtain structural information directly from the heat flux radiation emitted by the sample. Indeed, structral information can be retrieved by deconvolution of the IR spectral domain showing the vibrational bands associated with molecular units or structural groups within the material at a given temperature. As for recent instrumental improvements, several advances have been made for different characterization techniques operating in various spectral ranges [9, 10, 11], in particular for what concerns X-ray tomography using syncrotron radiation for dynamical microstructural changes [12, 13, 14], reaching acquisition speeds in the order of seconds. Concerning FT-IR spectrometry, one of the rising methods is the Rapid Scan [15], now tested with QCLs (Quantum Cascade Lasers) [16] to reach an even higher acquisition speed (from tens of milliseconds to few microseconds). The main problem which originates by the use of a Rapid Scan technique in FT-IR is the possible spectral distortion of the signal due to the change in temperature between the beginning and the end of the measurement. The aim of this paper is to present a new optimized method to be employed in the real time study of materials during temperature transitions from the molten state or, more generally, in out of thermodynamical equilibrium regions to the low temperature solid phase. It will present the details to build an optimized time-resolved emissometer able to give access to the spectral domain where vibrational motions occuring in molten, glass or crytalline states induce signatures. This new possibility originates from the past efforts made to perform high temperature measurements at very high precision [17, 18] combined with Rapid Scan techniques which allow real time observation of the melt and fast data acquisition. Up to now, research has focused on high temperature regions [19] to determine the melting point [20] of materials to be used as a standard for calibration purposes [21, 22, 23, 24] as well as instrumental optimization [25] and phenomena observation but yet, no study merged the two aspects to observe microstructural changes and the overall melt behaviour in a wide range of temperatures. In this work, we will present the results for the Rapid Scan FT-IR emissivity measurements of alumina and silica samples, put at nearly 100 K above their melting point by laser heating, and show the evolution in temperature during the free cooling process. The properties of liquid and solid alumina have been already studied in a wide temperature range [26] and using infrared spectroscopy [27, 28] as well as during solidification [29] or melting [30]. In the case of silica, its various crystalline polymorphs [32] as well as its liquid and glassy state [33] and its high temperature state [31] have already been widely studied experimentally and also from a molecular dynamics simulation point of view [34, 35]. This selection of well known materials which present huge differences in terms of glass formation and solidification processes has been used to confirm the versatility of the technique proposed to investigate on a vast variety of materials. A comparison of spectra obtained on the samples with the new method and the classic ones at a similar temperature in the melt region has been performed. The reliability of the method has additionally been tested by simulating fictive data to validate the results and estimate the effect of spectral distortion caused by the use of Fourier Transform on data originating from an infrared source that changes rapidly over time. The level of error will be proven to be tolerable if optimized conditions of acquisition are fullfilled as shown in the next sections.

2 Methodology and experimental setup

2.1 Time-resolved emissivity: theoretical aspects

In order to properly investigate the dynamic processes which lead to change in microstructural properties of a material, a theoretical description of the measurement method as well as careful attention to data treatment is necessary since the rapid changes of temperature can cause spectral distortion. The new method is implemented in the infrared emissivity spectrometer developed at CEMHTI [17] and is based on the characterization of heat fluxes emitted by the sample by acquiring continuously interferograms (see fig.1). This update takes into consideration the sample constantly changing its temperature during its cooling. The first step is the aquisition of flux measurements originating from the background radiation, the flux emitted by a blackbody reference at a fixed temperature and the one coming from the heated sample. These measurements are not performed simultaneously but consecutively. As for the background surrounding the sample, it is assumed that the enclosure produces a blackbody radiation and is given by the relation:

$$F_B = F_0 + fP^{T_B} \quad (1)$$

where F_0 is a flux contribution external from the closure, f is the transfer function of the measurement system and P^{T_B} is the intensity emitted by a blackbody at background temperature T_B, given by the Planck function P^T:

$$P^T(\bar{\nu}) = \frac{C_1 \bar{\nu}^3}{e^{\frac{C_2 \bar{\nu}}{T}} - 1} \tag{2}$$

with $C_1 = 2hc^2$ and $C_2 = \frac{hc}{k}$, $\bar{\nu}$ is the wavenumber and T is the temperature. Similarly, the flux signal aquired from the blackbody reference at a temperature T_R is given by:

$$F_R = F_0 + fP^{T_R} \tag{3}$$

Both of these flux measurements suffer no change in temperature during the aquisition process. As for the flux emitted by the sample, the situation is different from an equilibrium measurement since a time dependence in temperature T(t) becomes mandatory in the Planck function and reflects itself in the flux measurement given by:

$$F_S(t) = F_0 + f(\epsilon^{T(t)} P^{T(t)} + \rho^{T(t)} P^{T_B} + \tau^{T(t)} P^{T_B}) \tag{4}$$

Note that in the previous equation and in what follows, the spectral dependence of the physical quantities is omitted for the sake of simplicity. In this time changing case, the temperature (and consequently, time) dependence is present in the hemispherical directional spectral reflectance ($\rho^{T(t)}$) and transmittance ($\tau^{T(t)}$) of the sample as well as in the normal spectral emittance $\epsilon^{T(t)}$ [36, 37]. The Kirchhoff law and energy balance $\epsilon^{T(t)} = 1 - \rho^{T(t)} - \tau^{T(t)}$ can still be used to simplify the relation if the sample will still possess a given temperature at a given time, a necessary prerequisite since temperature has to be defined during the cooling:

$$F_S(t) = F_0 + f(\epsilon^{T(t)}(P^{T(t)} - P^{T_B}) + P^{T_B}) \tag{5}$$

However, this is true only up to a certain point because it is impossible to capture instantaneously the N points of the corresponding interferogram. Since the thermal flux will change during the time interval (Δt) of the acquisition, what is really measured is a composite interferogram ($I^*_{\Delta t}$). Each recorded point ($I_{i,i}$) displayed in figure 2 corresponds to the value taken by the interferogram of the flux emitted from the sample at a particular time ($t_i = (i-1)\Delta t/(N-1)$), at a particular path difference and at a specific temperature (T(t_i)). Therefore, the serie of N points obtained during a complete scan (I*) do not coincide with a conventional interferogram of a constant source. It is a set of values that correspond to the diagonal elements of a square matrix composed by the NxN points of a set of N interferograms. Up to here, the discussion has been theoretical, we will show in the next section the conditions and how to transform the composite interferogram to obtain a reliable estimation of the characteristic emissivity of the sample corresponding to the small time interval of the measurement. As the heat flux measurements performed are stored as interferograms, the last step to compute the spectral emittance is given by:

$$E_T = \frac{FT(I_S - I_B)}{FT(I_R - I_B)} \frac{P^{T_R} - P^{T_B}}{P^{T(t)} - P^{T_B}} E_R \tag{6}$$

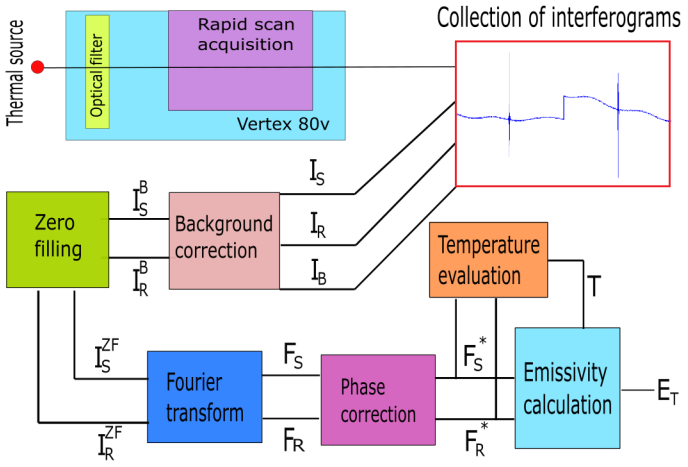

Figure 1: A graphical scheme of Rapid scan aquisition method and data treatment

where FT is the Fourier Transform and I_x are the interferograms of the fluxes originating from the sample (S), the blackbody reference (R) and the instrumental background (B), and E_R is the emissivity of the blackbody reference. The previous equation illustrates spectral emittance as the ratio of the sample spectral intensity and a same temperature blackbody spectral intensity (by definition) in a background corrected form [17]. The FT allows to retrieve the fluxes, which were previously background corrected (refer to fig.1 for the complete scheme):

$$E_T = \frac{F_S - F_B}{F_R - F_B} \frac{P^{T_R} - P^{T_B}}{P^{T(t)} - P^{T_B}} E_R \tag{7}$$

Since the sample used is opaque in the IR range we can retrieve the spectral reflectivity simply by:

$$R_T = 1 - E_T \tag{8}$$

2.2 Simulation test of the data analysis chain

Following the above theoretical description, numerical simulations have been performed to practically evaluate the impact of source of errors related to temperature variations during data acquisition and processing. Indeed, as we acquire data at different times, the interferograms might not reflect the sample at a fixed temperature but during time intervals depending on the speed of the mirror. These time intervals would reflect onto temperature intervals of different magnitude fixed by the speed of cooling. Hence the acquired signal would consist of a mixture or an average of the flux emitted by the material during the mirror's displacement time window, making the technique possibly unsuitable for our purpose. The previous problems have been quantified by numerically simulating all the steps involved in data processing, starting from the generation of a fictive material emissivity, modeled with a 2 phonon model in the interval 400-1600 cm^{-1}. The emissivity spectrum was chosen to be

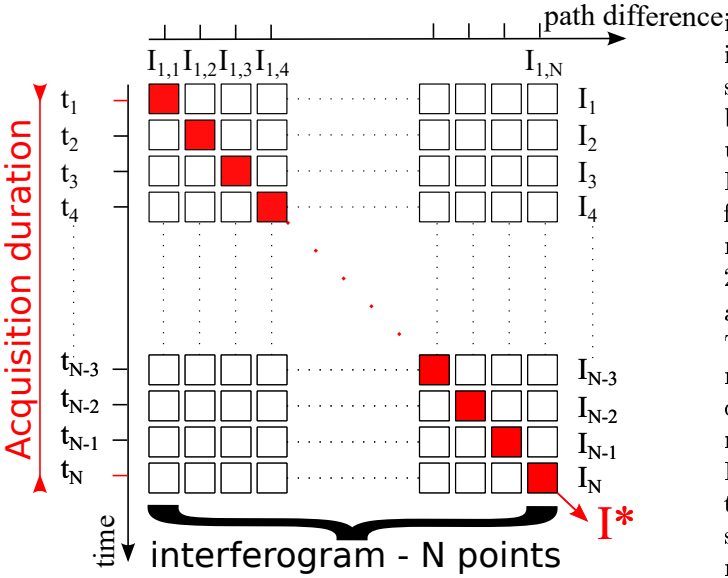

Figure 2: Scheme of the composite interferograms during the acquisition

similar to the ones observed in the molten state of non conductive materials. Two phonons contributing to the dielectric function are chosen to have a transversal frequency ω_{TO_j} of 600 and 1100 cm^{-1} and a damping γ_{TO_j} of 80 and 120 cm^{-1} and the dielectric strengths $\Delta\epsilon_j$ are set at 0.5 and 1, respectively. The choice of these values mimic real silica IR data and they take place in the Lorentz model of the dielectric function, expressed in the following formula:

$$\epsilon(\omega) = \epsilon_\infty + \sum_j \frac{\omega_{TO_j}^2 \Delta\epsilon_j}{\omega_{TO_j}^2 - \omega^2 - i\omega\gamma_{TO_j}} \tag{9}$$

The high frequency dielectric constant ϵ_∞ is set at 3, respecting the values typical of these materials. From this, it is possible to retrieve the emissivity and the reflectivity by using:

$$E(\omega) = 1 - R(\omega) = 1 - \left| \frac{\sqrt{\epsilon(\omega)} - 1}{\sqrt{\epsilon(\omega)} + 1} \right|^2 \tag{10}$$

In this way, the fictive data mimics the experimental one and it will go through the same data processing. The first step in the simulation is the generation of a set of composite interferograms having N points (with values compatibles to the 2^P factor used in FT) corresponding to temperature differences which can be also encountered in the experimental data. The N points also respect the standard conditions for points aquisition at a specific resolution, changeable by the user. The resolutions tested are the ones also used to determine the best conditions during the experiment and are the usual ones used for high temperature measurements (16, 8 or 4 cm^{-1}) since other values would provide no advantages. The temperature decrease between the recording of the first and last point of the interferogram is linear by hypothesis, which is a fairly good approximation given their temporal proximity of 0.05 s (time of a single scan) that corresponds to a temperature change less than 50 K in the worse investigated experimental conditions so the linear approximation is sufficient for such small temperature change. The maximum experimental quenching rate obtained with the presented technique is found to be 841 Ks^{-1}, a value comparable to aerodynamic levitation (typical order: 500 Ks^{-1} [38] up to 1000 Ks^{-1}[39]) and water quenching (maximum 153 Ks^{-1}[40], depending on water temperature) but still very far from splat quenching typical values (10^{10} Ks^{-1} [41]). To model our experiment, the highest temperature was set at 2500 K, the maximum temperature difference ΔT at 50 K, and the temperature steps each $\frac{(n-1)\Delta T}{N-1}$ with n from 1 to N. The choice of these values is made to encompass conditions met during measurements. The spectral distortion is higher during faster temperature changes i.e. at the fastest cooling rates observed experimentally (841 K/s for Al_2O_3 and 696 K/s for SiO_2) so a upper limit of 1000 K/s was chosen for the simulation to cover all situations. This translates onto setting $\Delta T_{max} = 50K$ for a measurement (Δt=0.05 s). Each numerical composite interferogram is evaluated by extracting the I_{ii} elements of the NxN dimensional matrix I_{kj} corresponding to specific acquisition conditions (temperature, cooling rate, aquisition speed and resolution). These data allow to compute the associated flux within the limits of the Nyquist frequency ($\omega_{max}/2$ where ω_{max} is the instrumental wavenumber limit) by applying the Fourier transform. In order to do this, a conversion from the standard N points to wavenumbers is performed within the details of the chosen resolution by using:

$$\Delta\nu = \frac{1}{N\Delta x} \tag{11}$$

and

$$\omega_{max} = \frac{N}{2}\Delta\nu \tag{12}$$

This conversion is the same performed by the Discrete Fourier Transform which is used to go from an interferogram to a spectrum. Apodisation using a Blackman Harris 3 terms [42], spectral ordering and zero filling to the next power of 2 is performed before using a Fast Fourier Transform (figure 1). The interferograms need to be corrected to eliminate their asymmetry produced by the acquisition of data points during a timeframe when the sample is dynamically changing its temperature. This intrinsic asymmetry is the cause of a complex FT output. For this reason, at this point we perform phase correction to eliminate the asymmetry of the interferogram and obtain a physical flux (real function). The type of phase correction performed on the data is the Mertz method [42] and is compiled to extract the amplitude spectrum from a complex output. Let us consider a common FT transformed interferogram $S(\nu)$:

$$S(\nu) = A(\nu)exp(i\phi(\nu)) \tag{13}$$

where A is the amplitude spectrum and the complex exponential apply to the phase function (ϕ). The extraction of A can be performed by taking the real part of the product of $S(\nu)$ and the inverse of the phase exponential, as seen in:

$$A(\nu) = Re[S(\nu)exp(-i\phi(\nu))] \tag{14}$$

In our case, A is the phase corrected signal which constitutes a kind of average thermal flux emitted by the sample

Error estimation (%)		
R	Error at 0 K/s	Error at 1000 K/s
16	0.8	1.2
8	0.4	0.6
4	0.2	0.3

Table 1: Error estimation at different resolutions (R) and for exact and highest cooling speed measurements

during the time of acquisition of the composite interferogram. This standard data processing is routinely performed on all kinds of FT-IR data to correct the spectral artifacts originating from the usage of a discrete transformation [42]. The fluxes have then been processed into emissivity data by taking into consideration that the emission reaches one at the Christiansen wavenumber so it can be used as a reference point to compute emissivity spectra, completing the entirety of data processing steps. This last point will be explained in more details in section 2.4. The first source of error is the interferogram distortion caused by the fast changes in sample temperature and its structure being out of equilibrium and changing rapidly, as explained previously. Figure 3 illustrates the highest time-induced deviation case: the cooling rate is maximum and the resolution is the lowest. Even in this case, the deviation is not as important and it does not prevent good data acquisition. Moreover, after phase correction, the relative error due to the interferogram distortion is estimated as being less than 0.04% from the highest to the lowest temperature reached during the acquisition process (see fig.4). So the application of the Mertz method is enough to account for it. For our setting, the cumulative error when performing a conventional measurement is estimated to be 2% [17] so the supplementary contribution due to the interferogram distortion we encountered is not a major contribution. As the simulation has been performed using different resolution values, it is also possible to quantify the impact of this parameter which is the main source of error (<1.2%) but it is still acceptable as seen in the second graph of figure 5 which illustrates the emission curves deviation due to resolution when compared to the exact one. Table 1 presents the error estimation from the analysis of the computed data.

It is also expected that almost all the smooth features present in the spectra are acquired at times close to the moment when the mirror finds itself placed at the zero path difference, thus avoiding possible artifacts and meaning that the computed (measured) spectra reflect an image of the sample in a brief time window, making the observation in real time at a specific temperature that is the average temperature during the Δt time interval. The best parameters to perform the measurements are discussed in section 2.4.

2.3 Experimental setup

The original experimental setup has already been described in details in [17] so it will be presented briefly here before introducing the additional improvements. A blackbody reference (PYROX PY8) and a heating apparatus based on a

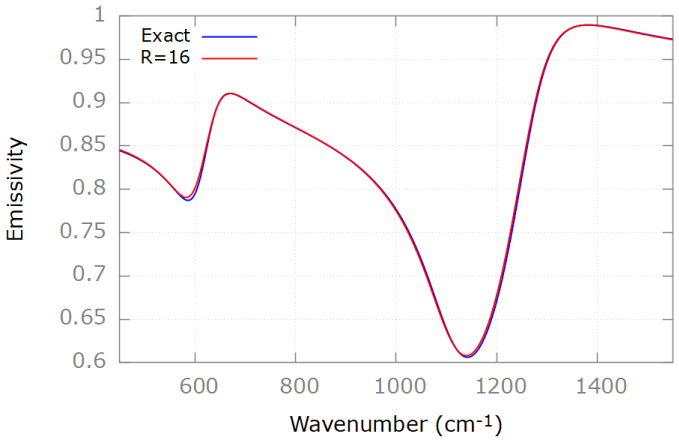

Figure 3: Exact (R=0) emissivity curve (blue) and the computed one (red) with a cooling rate of 1000 K/s at R=16 cm^{-1}.

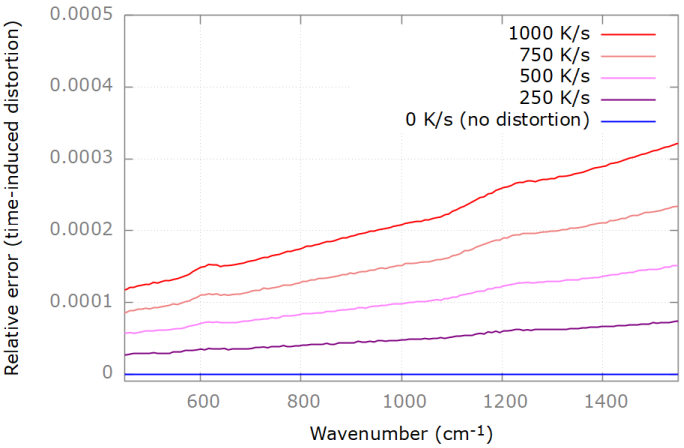

Figure 4: Emissivity relative error due to time-induced distorsion during the acquisition of a scan obtained by data simulated at different cooling rates

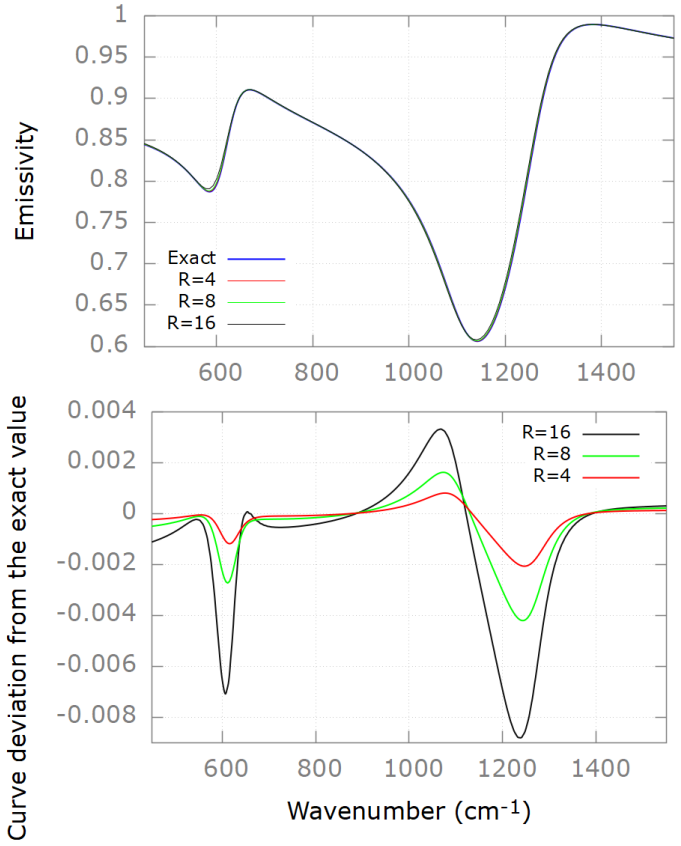

Figure 5: Effect of resolution on the emissivity spectrum

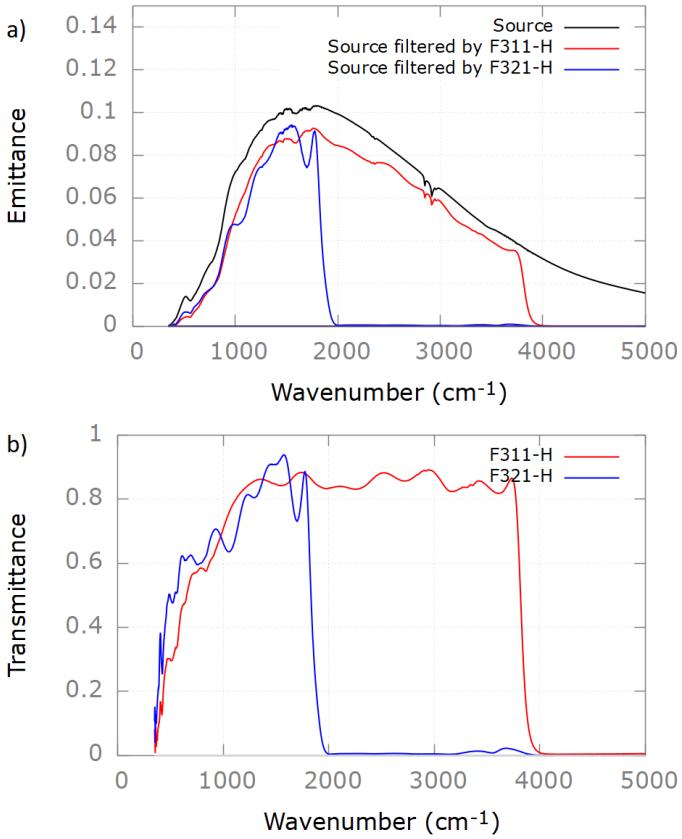

Figure 6: a) Emittance measurement with (S) and without filtering (S_{ref}). b) Retrieved transmittance (S/S_{ref}) of the filters used to limit the aquisition range (DLaTGS/KBr detector, Ge/KBr beamsplitter, tungsten lamp source)

CO_2 laser system (Coherent E400) are placed on a turntable (Aerotech ALAR-150) inside a purged enclosure. The design of the system ensures a constant and local heating of the sample even during motion of the turnable. The large diameter (12 mm at $1/e^2$) of the gaussian laser beam and the setting at 1 mm of the measurement aperture are enough to guarantee temperature homogeneity inside the spot during flux acquisition. The turntable makes possible the positioning of the sample and the reference at the focus points of the single path optical system which recollects the fluxes. The main difference between the previously presented layout and the one used in this study is that the CO_2 laser beam does not get split in two paths: the heating is performed unidirectionally by the usage of a mirror replacing the beamsplitter inside the enclosure. The in-depth thermal gradient induced by this unidirectional laser heating can be neglected in our case since the flux emitted in the considered spectral range comes from a very thin sample layer of few tens of micrometers under the air/sample interface. Therefore, the sample temperature is assumed to be constant within the probed volume. This configuration also allows using the sample as a self container for the molten bath, as explained in the next section. Moreover, the original layout has been improved by extending the UltraScan interferometer of the Bruker VERTEX 80v spectrometer. The new setup allows a faster data acquisition by increasing the speed of the moving mirror set inside the Michelson interferometer. The use of a Rapid Scan technique at the highest acquisition speeds causes a need to limit the spectral range of acquisition. Since the extreme temperatures induce thermal radiation in a very wide spectral range, it is thus mandatory to remove the contribution that is outside the range of interest to avoid signal aliasing [42] during the Fourier transform computation. To block the unwanted radiation, optical filters (F311-H or F321-H) are included in the optical path inside the Vertex spectrometer (see fig.1). The use of these filters allow to reduce the acquisition bandwith below 2000 cm^{-1} or 4000 cm^{-1} (see fig.6) and theoretically to enhance temporal resolution. In this study we employed an F311-H and set the Nyquist frequency at 3950 cm^{-1} since no significative change in acquition time was observed by reducing the Nyquist frequency below 2000 cm^{-1}. Additional electronic low-pass filters have been tested (5, 10 and 20 kHz) to improve acquistion. To cover the whole spectral range of vibrational motions, the use of 2 detectors is necessary. A KBr/DLaTGS (Bruker D301) is used to cover the 400 to 2000 cm^{-1} range while the 100 to 600 cm^{-1} is acquired with a Bolometer. The beamsplitters used are a Ge/KBr and a Mylar multilayered one, respectively. As the two measurements are not performed simultaneously, it is important that the experimental conditions are kept the same to assure reproducibility so a complete spectrum will be obtained by merging the two spectra in the acquisition region common to both detectors.

2.4 Sample preparation and measurement procedure

The samples were prepared by using pure alumina (99.999%) powder produced by Strem Chemicals and a 2mm thick silica glass supplied by UQG Optics. The use of a press operated at 8 tons allowed to produce circular alumina pellets with 13 mm of diameter and various thicknesses, ranging from 5 to 7 mm. The aim of this is having thicknesses which are sufficient to self contain a molten pool created by laser heating the sample from above (the depth of the molten pool will determine the amount of liquid and the length of the plateau, if present). The samples were heated up to 100 K above the melting point by the use of a CO_2 laser, thus creating a pool of molten material in the center of the pellet (around 8 mm of diameter). As the desired temperature is reached, the laser power is shutdown to allow the free cooling phenomenon to be observed by the continuous acquisition of the forwards and backwards interferograms which account for the heat flux originating from the sample. In order to obtain the emissivity or reflectivity spectra, a program has been developed. The input data are the interferograms of the sample, the reference set at 1280 K and the background at room temperature (295 K). Since we focus on oxide ceramics and glasses the real temperature of the sample can be directly computed by using the Christiansen point of the material because at this peculiar wavelength the emissivity of the material is comparable to the one of a blackbody [43, 44]. To extend the study to other materials like metals, the sample temperature can be monitored using an additional thermometer like a pyroreflectometer [45]. In our case, the studied materials possess this feature and the high reliablity of this physical property is beneficial. The temperature dependence of the point was taken into account by allowing the program to automatically search for the Christiansen point into a range (960-1040 cm^{-1} for Al_2O_3 and 1240-1320 cm^{-1} for SiO_2) and the emissivity value is fixed at 0.998. The wavelength range can be modified freely by the user and in this case it was set to take into account the temperature shift commonly observed for the material. The number of spectra acquired for the blackbody reference and the background was set to 1024 to allow a high signal to noise ratio and the sample is scanned 1000 times to be able to cover a wide temperature range. The data is visualized and processed with the OPUS software. Several tests have been performed to find the best compromise between aquisition speed and data resolution in order to be able to perform successively a structural analysis on the liquid phase and the undercooling region, completing the observation of the ongoing changes from the melt to the solid phase. The best parameters to perform this measurement, with a DLaTGS detector, are found to be 80 kHz for the acquisition speed, a resolution of 16 cm^{-1} and 2 scans (forward-backward) at each mirror movement, allowing the acquisition up to 20 spectra per second. Due to the high acquisition speed, the technique can be employed to study fast phenomena. The choice of these parameters was crucial to optimize the method for the particular aim of the study. Other configurations are possible, depending on the purpose of the study: by lowering the acquisition speed, it is possible to use higher resolutions to improve the quality of the spectra. Obviously this is convenient at lower temperatures where the cooling rate is not very high (in our case, 4.2 K/s at 500 K compared to the maximum observed in the range from 2400 K to 2050 K of up to 841 K/s). A good DLaTGS configuration for these cases is 40 kHz for the acquisition speed, a resolution of 8 cm^{-1} and 2 scans at each mirror movement. The Bolometer is able to reach a measurement speed of 160 kHz so it is possible to acquire twice the number of spectra during the same timeframe as DLaTGS (when the other parameters are in the same conditions). An MCT detector (D316) had also been tested and, thanks to the 100 times higher detectivity compared to the DLaTGS, 160 kHz was reached but it is unsuitable for our study since its low limit acquisition starts at 700 cm^{-1} so a lot of microstructural information would be missing, possibly denying a complete characterization. In any case, it could be perfectly used in case the desidered range is within its limits and it allowed us to further test the technique using a different detector. The main features of the detectors can be found in table 2.

Detectors specifics			
	DLaTGS	Bolometer	MCT
Spectral range (cm^{-1})	350-4000	10-500	700-7500
Detectivity (logD*[cm HZ/W])	8.7	11.5	10.5
Maximum speed (kHz)	80	160	160

Table 2: Specifics of the tested detectors

The purpose of this preliminary study was multiple: i) studying the fastest temperature changes, since the laser is shutdown so the temperature difference will be elevated, ii) searching for the best instrumental parameters to employ the method and iii) identify possible sources of distortion and errors in order to obtain reliable data. To summarize, the possible performances of the setup are various and it allows to study fast occurring phenomena and unquenchable phases by reaching a maximum acquisition speed of 20 spectra per second and a maximum temperature of almost 2700 K.

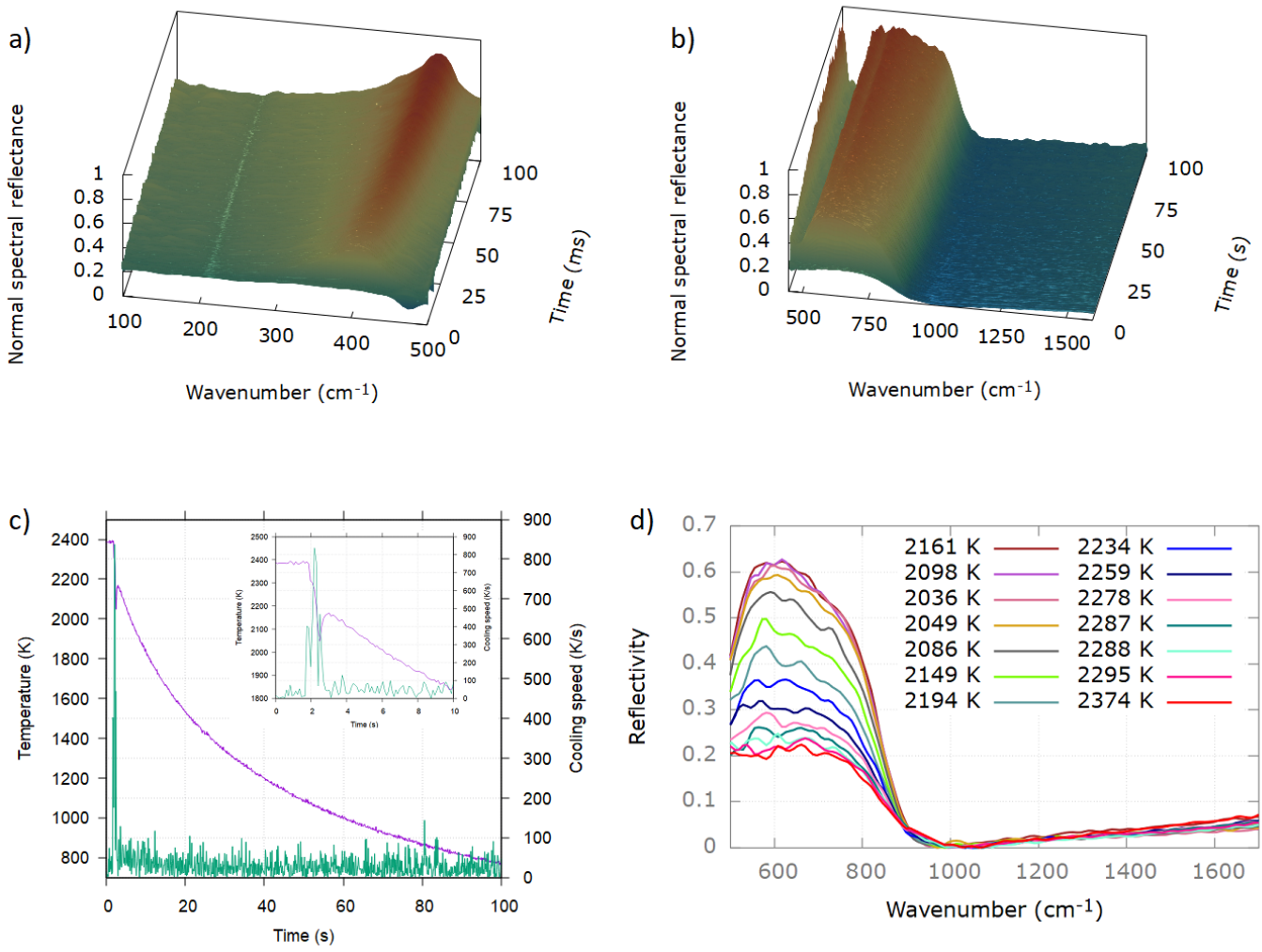

Figure 7: a) Reflectivity of Al_2O_3 in the waverange 100-500 cm^{-1}; b) Reflectivity of Al_2O_3 in the waverange 450-1600 cm^{-1}; c) Cooling curve (violet) and cooling speed (green) of Al_2O_3. Zoom on the undercooling region; d) Spectra acquired in the undercooling region of Al_2O_3, starting from the liquid and reaching solid phase

3 Results

3.1 Real time FT-IR measurements following the cooling of alumina and silica

The performance of the method was tested on alumina and silica samples. In the case of Al_2O_3 the observed phenomenon is crystallization of the undercooled melt onto the stable solid form of α-Al_2O_3, whilst SiO_2 vitrified. The a) and b) part of figure 7 and a) in figure 9 present the reflectivity data, while c) in 7 and b) in 9 show the temperature vs time of the previous data, with each point corresponding to the temperature extracted from each spectrum. d) in 7 and c) in 9 present a selection of spectra amongst the ones acquired. The process for spectra extraction still remains the same as the one performed in classical conditions: the main differences from the classic conditions are the number of spectra and the difficulty originating from a temperature dependence of the Christiansen point which shifts in wavenumber. This poses an obvious problem in temperature determination but since the tested materials have well known properties, the shift was taken into account by using an automatic search algorithm of the maximum emittance wavenumber during data processing. The spectra acquired while the laser was still on obviously present the CO_2 laser peak at 943 cm^{-1} and have been corrected to account for it by generating a straight line between 920 and 960 cm^{-1}. It is important to remark that the speed reached is enough to capture the undercooling zone as well as the cooling process, which have different results depending on the nature of the sample. The choice of showing different data sets was made to highlight the undercooling region in d) (maximum time 1 s, up to 20 spectra acquired) and show the transformation from liquid to solid for what concerns Al_2O_3, corresponding to the zoomed in part that can be seen in the inset of c) (figure 7). In this case, the spectra presented correspond to a small part of the total acquisition yet the most important since it illustrates a fast and metastable phenomenon. Full spectra combining the alumina data acquired by the two detectors are presented in fig.8. The data is acquired in middle infrared (MIR) and far infrared (FIR) because those contain all the signatures of vibrational motions and thus this is the spectral region of interest to study structural modifications from solid to liquid. As for SiO_2 the entire cooling spectra is shown in c) (figure 9) obviously with gaps to allow the eye to distinguish the evolution in temperature as an in situ measurement of the vitrification process. In this case, an additional measurement in FIR is not as necessary since the structure of silica is fully analyzable just by using the MIR one.

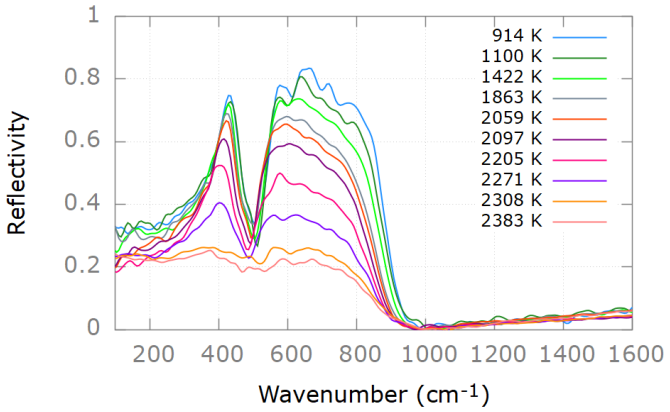

Figure 8: Merging of Al_2O_3 spectra acquired with the two detectors

3.2 Reliability

In order to show the reliability of the technique, high temperature classical measurements were conducted to be able to compare and validate the results obtained (figure 10). The spectra acquired in real time present obviously an higher signal-to-noise ratio but it does not pose a big problem in the global spectrum as the quality is enough to perform spectra decomposition for structural studies. The experimental conditions for the two sets are kept the same, as well as the samples used and the laser parameters to achieve a very close temperature for comparison. The data processing has also been the same. The only difference is the acquisition parameters being the standard classical one compared to the best choice made for DLaTGS at high temperatures. Other optimal parameters to perform Rapid Scan were also tested and the same result has been obtained but it would be pointless to present them due to the purpose of this test being an equilibrium measurement which must use the same parameters employed in the dynamical study (as well as in the data illustrated previously). The measurements were conducted at 5 kHz, 64 scans were averaged and the acquisition time is more than 1 min in classic conditions and, as for Rapid Scan, the parameters changed to 80 kHz, 2 scans and 0.1 s to complete the acquistion. The doubled time is due to the averaging of a backward and forward scans to have a proper spectrum which is still representing the conditions in which the technique can be used as the sample, in this case, is left in a static situation to perform our comparison. Spectra averaging is not convenient during the dynamical measurement due to the obvious doubling of the acquisition time, but as the cooling rates become slower at lower temperatures, it will provide higher quality data with a not as important spectral loss. It is of fundamental importance to state that this test had the purpose of providing a comparison to further prove the reliability of spectra acquired at the same temperature in the liquid which is, in this case even during Rapid Scan acquisition, acquired in equilibrium conditions before the laser shutdown.

3.3 Additional measurement possibilities and spectral analysis

The presented spectra have been acquired during the free cooling of the samples but the technique has the possibility of being extended to allow the performance and observation of phenomena at different cooling speeds. Indeed, the laser heating system can be considered as a "controllable temper-

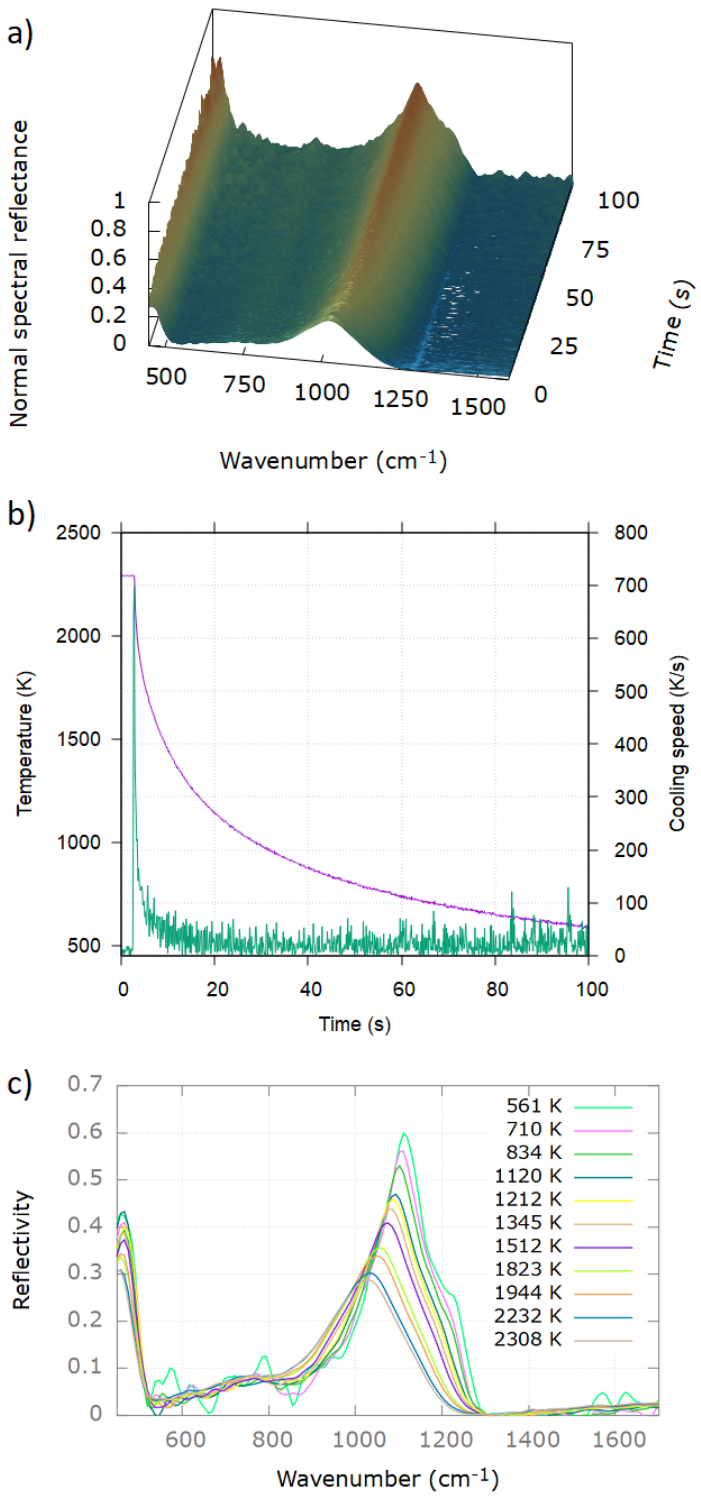

Figure 9: a) Reflectivity of SiO_2 in the waverange 450-1600 cm^{-1}; b) Cooling curve (violet) and cooling speed (green) of SiO_2; c) Spectra acquired during the cooling of SiO_2

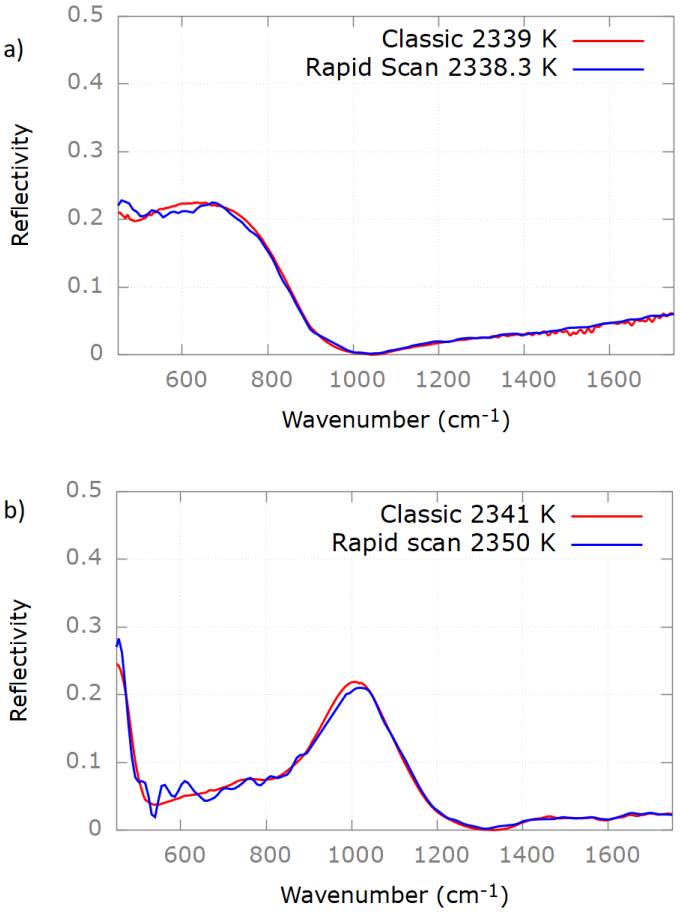

Figure 10: Spectra comparison of molten a) Al_2O_3 ,b) SiO_2

ature provider", meaning that the changes in temperature can be controlled directly by it so also the cooling rate and the relaxation time given to the sample. In other words, the temperature and the timeframe of the heating can be directly decided by operating the laser, allowing the user to decide how fast and how long the heating and the cooling needs to be performed. The laser used is capable of sustaining 500 W so it is possible to reach higher temperatures (in this experiment the output laser power was approximally 120 W). The maximum temperature reachable with this setting depends also on the thickness of the sample. A brief analysis is performed on a few reflectivity spectra of Al_2O_3 to highlight the evolution of the imaginary part of the dielectric function which is important to evaluate and distinguish the (group) vibrations. The acquisition of a spectral range enough wide to contain all phonon contributions allows also the use of Kramers-Kronig relations [46] to perform this data analysis (fig.11).

4 Conclusion

The development of a new methodology to observe fast phenomena in a wide range of temperatures has been described. The setting is able to acquire up to 20 spectra per second and reach a maximum sample temperature of 2700 K. Mul-

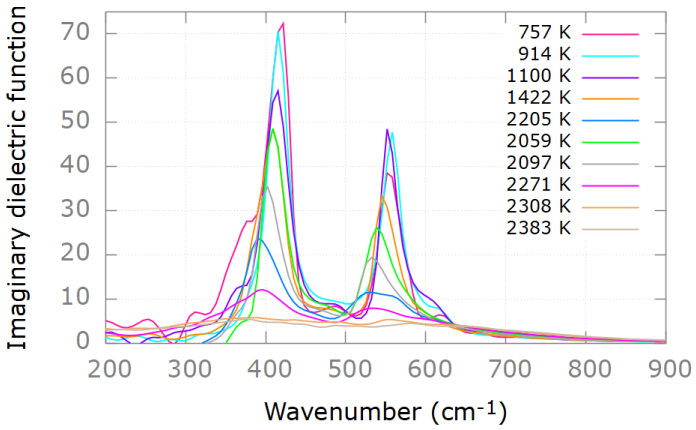

Figure 11: Imaginary dielectric function evolution of Al_2O_3 using Kramers-Kronig method

tiple tests have been performed to prove the reliability of the method. Out of equilibrium real time data from 100 to 1600 cm^{-1} acquired during solidification of molten samples has been illustrated for the first time. The example of Al_2O_3 illustrates the possibility to capture in-situ structural and dynamic information for out-of-equilibrium or metastable states, allowing a complete monitoring of the solidification process up to the final solid phase. SiO_2 highlights the potential of the technique to study the vitrification process of more complex liquids such as industrial glass compositions.

Conflict of interest
There is no conflict of interest

References

[1] K. Hashimoto, V. R. Badarla, and T. Ideguchi, 'High-Speed Fourier-Transform Infrared Spectroscopy with Phase-Controlled Delay Line', Laser & Photonics Reviews, vol. 15, no. 1, p. 2000374, 2021, doi: 10.1002/lpor.202000374.

[2] S. J. Parikh, B. J. Lafferty, and D. L. Sparks, 'An ATR-FTIR spectroscopic approach for measuring rapid kinetics at the mineral/water interface', Journal of Colloid and Interface Science, vol. 320, no. 1, pp. 177-185, Apr. 2008, doi: 10.1016/j.jcis.2007.12.017.

[3] M. Wang, K. Tashiro and Y. Ozaki, 'Reinvestigation of the β-to-α Crystal Phase Transition of Poly(butylene adipate) by the Time-Resolved X-ray Scattering and FTIR Spectral Measurements in the Temperature-Jump Process', Macromolecules, vol. 50, no. 10, pp. 3883-3889, 2017

[4] K. Golabek, K. Tarach, and K. Góra-Marek, 'Standard and rapid scan infrared spectroscopic studies of o-xylene transformations in terms of pore arrangement of 10-ring zeolites: 2D COS analysis', Dalton Transactions, vol. 46, no. 30, 2017, doi: 10.1039/c7dt00644f.

[5] G.N. Greaves, M.C. Wilding, S. Fearn, D. Langstaff, F. Kargl, Q. Vu Van, L. Hennet, I. Pozdnyakova, O. Majérus, R.J. Cernik, C. Martin, 'In situ structural studies of alumina during melting and freezing', Advances in Synchrotron Radiation, vol. 2, pp. 135-149, 2008

[6] L. Hennet et al., 'Application of time resolved x-ray diffraction to study the solidification of glass-forming melts', High temperatures-High pressures, vol. 40, pp. 263-270, 2011.

[7] P. Florian et al., 'Structure and dynamics of high-temperature strontium aluminosilicate melts', Physical chemistry chemical physics : PCCP, vol. 20, no. 44, pp. 27865-27877, 2018, doi:10.1039/c8cp04908d

[8] P. Florian, D. Massiot, B. Poe, I. Farnan and J.P. Coutures, 'A time resolved 27Al NMR study of the cooling process of liquid alumina from 2450 °C to crystallisation', Solid State Nuclear Magnetic Resonance, vol. 5, no. 3, pp. 233-238, Dec. 1995, doi: 10.1016/0926-2040(95)01188-X.

[9] K. Hashimoto, V. R. Badarla and T. Ideguchi, 'Mid-infrared phase-controlled Fourier-transform spectroscopy', in Conference on Lasers and Electro-Optics (2020), paper STh3F.2, May 2020, p. STh3F.2. doi: 10.1364/CLEOSI.2020.STh3F.2.

[10] Q. Yang, 'Ultrahigh-resolution rapid-scan ultraviolet-visible spectrometer', OSA Continuum, OSAC, vol. 1, no. 3, pp. 812-821, Nov. 2018, doi: 10.1364/OSAC.1.000812.

[11] Y. Zhang, C. Cai, S.F. Pang, J. P. Reid, and Y.-H. Zhang, 'A rapid scan vacuum FTIR method for determining diffusion coefficients in viscous and glassy aerosol particles', Phys. Chem. Chem. Phys., vol. 19, no. 43, pp. 29177-29186, 2017, doi: 10.1039/C7CP04473A.

[12] O. Müller, M. Nachtegaal, J. Just, D. Lützenkirchen-Hecht, and R. Frahm, 'Quick-EXAFS setup at the SuperXAS beamline for in situ X-ray absorption spectroscopy with 10 ms time resolution', J Synchrotron Rad, vol. 23, no. 1, pp. 260?266, Jan. 2016, doi: 10.1107/S1600577515018007.

[13] Y. Wang et al., 'A high-throughput x-ray microtomography system at the Advanced Photon Source', Review of Scientific Instruments, vol. 72, no. 4, pp. 2062-2068, Apr. 2001, doi: 10.1063/1.1355270.

[14] M. Caselle et al., 'An ultra-fast data acquisition system for coherent synchrotron radiation with terahertz detectors', Journal of Instrumentation, vol. 9, p. C01024, Jan. 2014, doi: 10.1088/1748-0221/9/01/C01024.

[15] B. Süss, F. Ringleb, and J. Heberle, 'New ultrarapid-scanning interferometer for FT-IR spectroscopy with microsecond time-resolution', Review of Scientific Instruments, vol. 87, no. 6, p. 063113, Jun. 2016, doi: 10.1063/1.4953658.

[16] J. Schnee, P. Bazin, B. Barviau, F. Grisch, B. J. Beccard, and M. Daturi, 'Coupling a Rapid-Scan FT-IR Spectrometer with Quantum Cascade Lasers within a Single Setup: An Easy Way to Reach Microsecond Time Resolution without Losing Spectral Information', Anal. Chem., vol. 91, no. 7, pp. 4368-4373, Apr. 2019, doi: 10.1021/acs.analchem.8b04621.

[17] D. De Sousa Meneses, P. Melin, L. del Campo, L. Cosson, and P. Echegut, 'Apparatus for measuring the emittance of materials from far infrared to visible wavelengths in extreme conditions of temperature', Infrared Physics & Technology, vol. 69, pp. 96-101, Mar. 2015, doi: 10.1016/j.infrared.2015.01.011.

[18] P. C. Nordine, J. K. R. Weber, and J. G. Abadie, 'Properties of high-temperature melts using levitation', Pure and Applied Chemistry, vol. 72, no. 11, pp. 2127-2136, Jan. 2000, doi: 10.1351/pac200072112127.

[19] L. B. Skinner et al., 'Joint diffraction and modeling approach to the structure of liquid alumina', Phys. Rev. B, vol. 87, no. 2, p. 024201, Jan. 2013, doi: 10.1103/PhysRevB.87.024201.

[20] H. Reiss, I. B. Wilson,'The effect of surface on melting point', Journal of Colloid Science, vol. 3, no. 6, pp. 551-561, 1948, ISSN 0095-8522

[21] S. J. Schneider, 'Cooperative determination of the melting point of alumina', Pure and Applied Chemistry, vol. 21, no. 1, pp. 115-122, 1970

[22] T. Sata and T. Takahashi, 'Measurement of the Melting Point of Alumina by means of DTA', Journal of the Ceramic Association, Japan, vol. 79, no. 906, pp. 70-71, 1971, doi: 10.2109/jcersj1950.79.90670.

[23] R. F. Geller and P. J. Yavorsky, 'Melting point of alpha-alumina', Journal of research of the National Bureau of Standards, vol. 34, 1945.

[24] J. Coutures and M. Rand, 'Melting temperatures of refractory oxides - Part II: Lanthanoid sesquioxides', Pure and Applied Chemistry, vol. 61, pp. 1461-1482, 1989.

[25] M. Naji, D. De Sousa Meneses, G. Guimbretière, Y. Vaills, 'In Situ High-Temperature Probing of the Local Order of a Silicate Glass and Melt during Structural Relaxation', Journal of Physical Chemistry C, vol. 119, pp. 8838-8848, 2015.

[26] P. H. Zhang, R. Z. Chang, Z. Wei, H. Cao and X. N. Zhou, 'The melting point, latent heat of solidification, and enthalpy for both solid and liquid α-Al2O3 in the range 550-2400 K', International Journal of Thermophysics, vol. 7, pp. 811-819, 1986.

[27] M. Schubert, T. E. Tiwald, and C. M. Herzinger, 'Infrared dielectric anisotropy and phonon modes of sapphire', Phys. Rev. B, vol. 61, no. 12, pp. 8187-8201, Mar. 2000, doi: 10.1103/PhysRevB.61.8187.

[28] J. Y. Yang, M. Xu, and L. H. Liu, 'Infrared radiative properties of alumina up to the melting point: A first-principles study', Journal of Quantitative Spectroscopy and Radiative Transfer, vol. 184, pp. 111-117, Nov. 2016, doi: 10.1016/j.jqsrt.2016.07.006.

[29] V. Petrov and A. Vorobyev, 'Spectral emissivity and radiance temperature plateau of self-supporting alumina melt at rapid solidification', High Temperatures- High Pressures. vol. 35/36. pp. 321-329, 2003, doi: 10.1068/HTJR141.

[30] H. Sakate et al., 'Observation of Al_2O_3 melting and freezing plateaus using a cavity-type tungsten crucible' Metrologia, vol. 32, no. 2, p. 129, 1995.

[31] D. Huang, C. Guo, M. Zhang, and L. Shi, 'Characteristics of nanoporous silica aerogel under high temperature from 950°C to 1200°C', Materials & Design, vol. 129, pp. 82-90, Sep. 2017, doi: 10.1016/j.matdes.2017.05.024.

[32] I. G. Polyakova, 'The Main Silica Phases and Some of Their Properties', De Gruyter, pp. 197-268, 2014. doi: 10.1515/9783110298581.197.

[33] P. F. McMillan, B. T. Poe, P. H. Gillet, and B. Reynard, 'A study of SiO_2 glass and supercooled liquid to 1950 K via high-temperature Raman spectroscopy', Geochimica et Cosmochimica Acta, vol. 58, no. 17, pp. 3653-3664, Sep. 1994, doi: 10.1016/0016-7037(94)90156-2.

[34] B.Vessal, M. Amini, D. Fincham and C. R. A. Catlow, 'Water-like melting behaviour of SiO_2 investigated by the molecular dynamics simulation technique', Philosophical Magazine B, vol. 60, no. 6, pp. 753-775, 1989.

[35] J. Kubicki and A. Lasaga, 'Molecular dynamics simulations of SiO2 melt and glass: Ionic and covalent models', Am. Mineral., vol. 73, pp. 941-955, Jan. 1988.

[36] D. De Sousa Meneses, P. Melin, L. del Campo, O. Rozenbaum, and L. Cosson, 'Probing high temperature thermal emissive properties of energy materials and coatings with emission spectroscopy augmented by in situ reflection', Infrared Physics & Technology, vol. 108, p. 103329, Aug. 2020, doi: 10.1016/j.infrared.2020.103329.

[37] J. R. Howell, M. P. Menguc, and R. Siegel, Thermal Radiation Heat Transfer, 5th ed. Boca Raton: CRC Press, 2010. doi: 10.1201/9781439894552.

[38] P. Kidkhunthod, L. B. Skinner, A. C. Barnes, W. Klysubun, and H. E. Fischer, 'Structure of Ba-Ti-Al-O glasses produced by aerodynamic levitation and laser heating', Phys. Rev. B, vol. 90, no. 9, p. 094206, Sep. 2014, doi: 10.1103/PhysRevB.90.094206.

[39] M. Suzuki, H. Serizawa, and N. Umesaki, 'Phase Identification of Crystal Precipitated from Molten CaO-SiO_2-FeO_x-P_2O_5 Slag by High Temperature In-situ X-ray Diffraction', ISIJ Int., vol. 60, no. 12, pp. 2765-2772, Dec. 2020, doi: 10.2355/isijinternational.ISIJINT-2020-148.

[40] G. Totten, C. Bates and N. Clinton, 'Handbook of quenchants and quenching technology', Materials & Design, vol. 14, no. 6, p. 368, Jan. 1993, doi: 10.1016/0261-3069(93)90123-D.

[41] H. A. Davies, J. B. Hull, 'Some aspects of splat-quenching in an inert atmosphere and of the formation of non-crystalline phases in Al-17.3 at. % Cu, germanium and tellurium', J Mater Sci, vol. 9, pp. 707-717, 1974.

[42] W. Herres and J. Gronholz, 'Understanding FTIR Data Processing Part 1: Data Acquisition and Fourier Transformation 1', 2007.

[43] B. Rousseau, J. Brun, D. Meneses, and P. Echegut, 'Temperature Measurement: Christiansen Wavelength and Blackbody Reference', International Journal of Thermophysics, vol. 26, pp. 1277-1286, Jul. 2005, doi: 10.1007/s10765-005-6726-4.

[44] J. Manara et al., 'Long Wavelength Infrared Radiation Thermometry for Non-Contact Temperature Measurements in Gas Turbines', Infrared Physics & Technology, vol. 80, 2017, doi:10.1016/j.infrared.2016.11.014.

[45] D. Hernandez, A. Netchaieff, and A. Stein, 'True temperature measurement on metallic surfaces using a two-color pyroreflectometer method', Review of Scientific Instruments vol. 80, p. 094903, 2009, doi:10.1063/1.3208011.

[46] J.M. André, K. Le Guen, P. Jonnard, N. Mahne, A. Giglia, et al., 'On the Kramers-Kronig transform with logarithmic kernel for the reflection phase in the Drude model', Journal of Modern Optics, Taylor & Francis, 2010, vol. 57 (16), pp.1504. doi:10.1080/09500340.2010.506015